Gluonic radius of the proton and high energy $\overline{pp}$ scattering

M. Kawasaki*
Physics Department, Gifu University, Yanagido, Gifu 501-11, Japan

T. Maehara†
Faculty of School Education, Hiroshima University, Higashi-Hiroshima 739, Japan

M. Yonezawa
Faculty of Liberal Arts, Fukuyama University, Fukuyama 729-02, Japan

(Received 29 August 1997; published 24 December 1997)

The present experimental data of elastic $\overline{pp}$ scattering suggest that the asymptopia in the Chou-Yang picture for elastic hadron-hadron diffraction scattering may be nearly realized in the energy region of the CERN Super Proton Synchrotron and the Fermilab Tevatron Collider, $\sqrt{s}=0.5$–1.8 TeV. The analysis gives information on the root mean square radius of the gluon distribution in the proton ($\overline{r_g}\equiv\langle r^2_{gluon}\rangle^{1/2}_p$), which is estimated to be $0.87\lesssim\overline{r_g}\lesssim 0.95$ fm. [S0556-2821(98)01003-0]

PACS number(s): 13.85.Dz, 12.40.Nn, 14.20.Dh

I. INTRODUCTION

The diffraction interaction which exposes one important face of the strong interaction in the soft and semihard region has still much to be explored, even at the phenomenological level. Nearly three decades ago Chou and Yang [1] proposed an idea for the diffraction mechanism of elastic hadron scattering, that the interaction is caused by the absorption of one extended hadron passing through another extended hadron. This simple picture has stimulated interest in the geometrical aspect of the diffraction interaction [2]. The Chou-Yang model has been applied to hadron-hadron elastic scattering with some success in explaining certain basic features of the diffraction scattering, but later it met difficulties. The most serious one is that the model does not cope with the expanding feature of the diffraction interaction observed in the CERN Intersecting Storage Rings (ISR) energy region and at higher energies [3–5]. This difficulty, however, may be overcome if we generalize the original picture by taking two components, the quark and the gluon, having different energy behaviors as the constituents of the hadron.

In the high energy region from the CERN Super Proton Synchrotron ($Sp\overline{p}S$) to the Fermilab Tevatron Collider, $\sqrt{s}=0.5$–1.8 TeV, the experimental data of elastic $\overline{pp}$ scattering suggest that the opacity increases while the interaction radius remains nearly constant [4,5]. This shows that the asymptopia in the Chou-Yang picture for hadron-hadron diffraction scattering may be virtually realized in this energy region. The purpose of this paper is to give a more detailed account of the previous suggestion and to estimate the bounds for the gluonic extension of the proton from the differential cross section data of elastic $\overline{pp}$ scattering including the experiments by the collaboration group of the Collider Detector at Fermilab (CDF) [6,7].

*Electronic Address: kawasaki@cc.gifu-u.ac.jp
†Electronic Address: tmaehar@sed.hiroshima-u.ac.jp

II. EXPONENTIAL DIFFERENTIAL CROSS SECTION

Before we make a detailed analysis of the experimental data, it will be useful to examine the problem by assuming the differential cross section which decreases exponentially in the momentum transfer $|t|$. We neglect the contribution from the real part of the scattering amplitude. The imaginary part of the scattering amplitude $F(s,t)$ is written in the impact-parameter representation in terms of the real eikonal function $\Omega(s,b)$ as

$$\mathrm{Im}F(s,t)=\int_0^\infty db\, b(1-e^{-\Omega(s,b)})J_0(\sqrt{-t}b). \tag{1}$$

Here s is the squared total energy in the center of mass system, b the impact parameter, and J_0 the Bessel function of order zero. For the exponentially falling differential cross section with the logarithmic forward slope B, $\mathrm{Im}F(s,t)$ is given by

$$\mathrm{Im}F(s,t)=\frac{\sigma_{\mathrm{t}}}{4\pi}e^{Bt/2}, \tag{2}$$

with the total cross section σ_{t}. This gives the real eikonal

$$\Omega(s,b)=-\ln\left(1-\frac{\sigma_{\mathrm{t}}}{4\pi B}e^{-b^2/2B}\right)$$
$$=-\ln(1-4xe^{-b^2/2B}), \tag{3}$$

where x is the elasticity. The positivity requirement for $\Omega(s,b)$ imposes the restriction $x\leqslant 1/4$. Incidentally the CDF experiments at 1.8 TeV have given $x=0.246\pm 0.004$ [6,7], which is near the unitarity bound 1/4.

We denote the Fourier-Bessel transform of the eikonal $\Omega(s,b)$ by $\overline{\Omega}(s,t)$. Let us define

$$\overline{G}(s,t)\equiv\overline{\Omega}(s,t)/\overline{\Omega}(s,0). \tag{4}$$

TABLE I. Summary of the experimental data.

Experiment [Refs.]	$\sqrt{s}$ (TeV)	σ_t (mb)	ρ	x	B [(GeV/c)$^{-2}$]
UA4/2 [9–11]	0.541	62.2 ± 1.5	0.135 ± 0.015	0.215 ± 0.005	15.5 ± 0.1
CDF [6,7]	0.546	61.26 ± 0.93	0.15 [a]	0.210 ± 0.002	15.28 ± 0.58
E-710 [12,13]	1.8	72.8 ± 3.1	0.140 ± 0.069	0.230 ± 0.025	16.99 ± 0.47
CDF [6,7]	1.8	80.03 ± 2.24	0.15 [a]	0.246 ± 0.004	16.98 ± 0.25

[a]Assumed.

This is given in the case of the exponential cross section by

$$\overline{G(s,t)}=\frac{1}{\mathrm{Li}_2(4x)}\sum_{k=1}^{\infty}\frac{(4x)^k}{k^2}\exp\left(\frac{Bt}{2k}\right), \tag{5}$$

where Li_n is the polylogarithmic function of order n [8] defined by

$$\mathrm{Li}_n(z)=\sum_{k=1}^{\infty}\frac{z^k}{k^n}. \tag{6}$$

In the Chou-Yang-type geometrical picture the effective root-mean-square radius of the proton may be defined by

$$\overline{r^2}\equiv\langle r^2\rangle_p=3\frac{d}{dt}\overline{G(s,t)}\Big|_{t=0}, \tag{7}$$

which gives, for Eq. (5),

$$\overline{r^2}=\frac{3}{2}B\frac{\mathrm{Li}_3(4x)}{\mathrm{Li}_2(4x)}. \tag{8}$$

The experimental results from the UA4 Collaboration [9], the UA4/2 [10,11], and the CDF [6,7] at $\sqrt{s}=0.541$–0.546 TeV and the CDF [6,7] and the E-710 [12,13] at 1.8 TeV are given in Table I. The effective proton radius calculated by Eq. (8) from the experimental values of the elasticity x and the forward logarithmic slope B is given in Table II. The radius can be said, within the uncertainty of the experiment, to be independent of the energy, though the *naive* interaction range related to $\sqrt{B}$ definitely increases from $Sp\overline{p}S$ to Tevatron. The proton matter extension is larger than its electromagnetic radii 0.83–0.84 fm [14], suggesting that the dominant absorber is *not* the quark in this energy region.

Actually the differential cross sections of $\overline{pp}$ scattering have the dip-bump structure around $|t|\approx 1.0$ (GeV/c)^2 in this energy region and they show the exponentially falling cross section approximately only at small momentum transfers $|t|\lesssim 0.1$ (GeV/c)^2. Another point which differs from the exponential behavior is the curvature structure at small momentum transfers which changes as the total cross section increases from positive (concave) to negative (convex) in the geometrical model such as the Chou-Yang picture, although its details will, however, depend on the shape of the eikonal. This curvature structure will affect the determination of the forward slope B, which is usually performed by assuming a structureless forward peak. It is, therefore, necessary to examine the problem more carefully for the scattering amplitudes which reproduce details of the observed differential cross sections.

III. EVIDENCE OF THE CHOU-YANG ASYMPTOPIA IN THE ENERGY REGION FROM THE $Sp\overline{p}S$ TO THE TEVATRON

At high energies the elastic scattering amplitude is dominated by the imaginary part. However, the contribution from the real part cannot be neglected at small momentum transfer where the Coulomb interaction becomes appreciable as well as in the dip-bump region where the imaginary part becomes small, if a better description of the experimental data is attempted. In the present approach the real part is induced from the imaginary part by the derivative dispersion relation (DDR) [5,15]. We assume the dominance of the crossing-even amplitude for which the DDR gives

$$\mathrm{Re}F(s,t)\approx\frac{\pi s}{2}\frac{d}{ds}\mathrm{Im}F(s,t). \tag{9}$$

In practice we introduce the energy dependence of the imaginary part of the scattering amplitude through the eikonal $\Omega(s,b)$ by making an approximation as

$$\Omega(s,b)=w(s)g(b/\kappa(s)), \tag{10}$$

TABLE II. The effective proton radius calculated by Eq. (8) for the $Sp\overline{p}S$ and Tevatron experimental data for the elasticity x and the forward logarithmic slope B.

Experiment	$\sqrt{s}$ (TeV)	x [a]	B [(GeV/c)$^{-2}$]	r_{rms} [a] (fm)
UA4/2	0.541	0.215 (0.205)	15.5	0.864±0.021 (0.872±0.021)
CDF	0.546	0.210 (0.205)	15.28	0.862±0.018 (0.866±0.038)
E-710	1.8	0.230 (0.219)	16.99	0.890±0.054 (0.901±0.049)
CDF	1.8	0.246 (0.241)	16.98	0.864±0.022 (0.874±0.036)

[a]The figures in the parentheses are the elasticity $\sigma_t/(16\pi B)$ of the exponentially falling differential cross section and the corresponding radius.

TABLE III. The Chou-Yang-model fit to the experimental differential cross sections of $\bar{p}p$ scattering at 1.8 TeV by the S$p\bar{p}$S eikonal at 0.541–0.546 TeV [20]. The results of the GGS fit are also given.

Model	σ_t (mb)	B [(GeV/c)$^{-2}$]	x	ρ	w	w_d	κ	κ_d	χ^2/N_{DP} E-710	CDF	total
Chou-Yang	78.54	17.05	0.245	0.140 [a]	1.397	0.293	1 [a]	0 [a]	34.2/51	48.2/26	82.4/77
GGS	78.48	17.13	0.245	0.140 [a]	1.388	0.239	1.002	0.012	34.1/51	48.1/26	82.2/77

[a]Assumed.

where $w(s)$ and $\kappa(s)$ are functions depending only on s. This is essentially the generalized geometrical scaling (GGS) model [4,5].

With the expression (10) for the eikonal, the real part is given by Eq. (9) as

$$\mathrm{Re}F(s,t) = w_d\ \kappa^2(s)\int_0^\infty d\beta\,\beta g(\beta)e^{-w(s)g(\beta)}J_0(\kappa(s)\beta\sqrt{-t}) + \kappa_d\ \frac{2}{\kappa(s)}\ \frac{d}{dt}[t\mathrm{Im}F(s,t)], \tag{11}$$

where

$$w_d \equiv \frac{\pi s}{2}\frac{d}{ds}w(s), \qquad \kappa_d \equiv \frac{\pi s}{2}\frac{d}{ds}\kappa(s). \tag{12}$$

Here the second term on the right-hand side of Eq. (11) corresponds to the Martin formula [16].

Now let us define the asymptopia in the Chou-Yang picture as the energy region where the gluon becomes fully dominant [17]. Phenomenologically this can be seen if the relation

$$\frac{d\ln\Omega(s,b)}{ds} = f(s) \tag{13}$$

holds, $f(s)$ being a function depending on only the energy variable s. In the approximation (10) this is satisfied if κ is independent of energy. This is the Chou-Yang model in the factorized eikonal version [18,19].

The eikonal-shape function $g(\beta)$ of elastic $\bar{p}p$ scattering at $\sqrt{s}=$ 0.541–0.546 TeV can be evaluated from the scattering amplitude determined previously [20] for the UA4 [9,21] and UA4/2 [11] experiments. This eikonal (referred to as the S$p\bar{p}$S eikonal hereafter) is used to fit the differential cross section data at 1.8 TeV of the E-710 experiment [22] [the number of data points $N_{DP}=51$, $|t|$ = 0.034–0.65 (GeV/c)^2] and of the CDF experiment [6,7] [$N_{DP}=26$, $|t|$ = 0.035–0.285 (GeV/c)^2] at Tevatron. In the fit we take $\kappa=1$ and $\kappa_d=0$ corresponding to the Chou-Yang model and make the luminosities of the E-710 and the CDF experiment free. In total there are four free parameters in the fit: the values of $w(s)$ and $w_d(s)$ at $\sqrt{s}=1.8$ TeV for the scattering amplitude and two free normalization parameters for the experimental data. The parameter $w_d(s)$ enters in the evaluation of the real part by the derivative dispersion relation, Eq. (11). Here we assume the ratio of the real part to the imaginary part of the forward scattering amplitude $\rho=0.14$ [12].

The best-fit solution at 1.8 TeV is given in Table III and the differential cross section of this solution is shown in Fig. 1. In the CDF measurements there are four data points occupying more than half of the χ^2 value, $|t|$ = 0.035, 0.055, 0.245, and 0.255 (GeV/c)^2, contributing 26.9 to the χ^2 value. If these data are omitted, we have $\chi^2/N_{DP}=$ 21.3/22 for the CDF experiment, showing a good fit. The total and elastic cross sections σ_t and σ_{el} of this solution are 78.54 mb and 19.24 mb (the elasticity $x=0.245$), respectively. The forward logarithmic slope B is 17.05 (GeV/c)$^{-2}$. These values are in better agreement with those of the CDF experiment than the E-710 one as seen in Table I. The normalization factors are 1.16 for the E-710 and 1.01 for the CDF data, indicating a discrepancy of 15% between them.

In order to examine the stability of the interpretation by the Chou-Yang model with one component, we try an eikonal with $g(b/\kappa)$ by varying κ freely in fitting the experimental data as in the GGS model [4,5]. We have the best-fit solution having $\chi^2/N_{DP}=82.2/77$ which is given in Table III. The results differ very little from the Chou-Yang model with $\kappa=1.002$ and only small changes in other free parameters and predictions. The CDF cross sections imply a weaker energy dependence for κ than the E-710 data and we estimate that the change of κ is at most 1% from the S$p\bar{p}$S to the Tevatron. In the analyses by Block *et al.* [17], which were

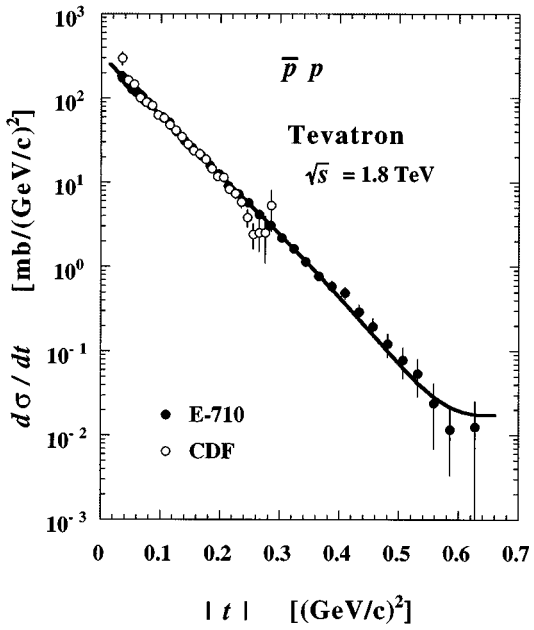

FIG. 1. The differential cross section of $\bar{p}p$ scattering at 1.8 TeV calculated by the S$p\bar{p}$S eikonal determined from the UA4 and UA4/2 experiments at 0.541–0.546 TeV [20].

TABLE IV. The predictions by the Chou-Yang model with the $Sp\overline{p}S$ eikonal at 0.541–0.546 TeV [20]. Here the input data for the calculation are σ_t and ρ.

	$\sqrt{s}$ (TeV)	σ_t (mb)	ρ	x	B [(GeV/c)$^{-2}$]	B/B_{MM}[a]	Opaqueness [b]
$Sp\overline{p}S$ [c]	0.541–0.546	62.2	0.118	0.210	16.1	1.18	0.419
CDF	0.546	61.26	0.15	0.209	16.0	1.18	0.416
E-710	1.8	72.8	0.140	0.234	16.7	1.16	0.449
CDF	1.8	80.03	0.15	0.249	17.2	1.15	0.464
		100.0	0.135	0.281	18.5	1.12	0.488
		105.0	0.133	0.287	18.8	1.12	0.491
LHC	14	110.0	0.133	0.294	19.2	1.11	0.494

[a]The MacDowell-Martin bound $B_{MM}\equiv(1+\rho^2)\sigma_t/18\pi x$.
[b]The central opaqueness defined by the impact-parameter amplitude at $b=0$: Its unitarity bound is 0.5.
[c]The results of the fit to the differential cross sections in Ref. [20].

performed before the UA4/2 and CDF experiments, the interaction radius expands over 2% in this energy interval, while our present results indicate a variation by less than 1%, signaling an even earlier onset of the asymptopia than that suggested by their results. Incidentally the growth of the interaction radius is about 7% between the CERN ISR and the $Sp\overline{p}S$, $\sqrt{s}=$ 0.06–0.55 TeV [4,5].

IV. PREDICTIONS AT THE LHC ENERGY REGION

The results in the previous section suggest the Chou-Yang asymptotic picture is nearly realized above the $Sp\overline{p}S$ region. It is, therefore, interesting to predict the differential cross section at higher energies on the basis of the $Sp\overline{p}S$ eikonal obtained at 0.541–0.546 TeV [20].

The necessary input data for the calculation in the energy region of the CERN Large Hadron Collider (LHC) are the values of σ_t (or σ_{el} or B) and ρ. The present theoretical predictions for the total cross section in the LHC region still have a considerable uncertainty [23]. We tentatively take 110 mb as the total cross section at 14 TeV. As for the ratio of the real part to the imaginary part of the forward scattering amplitude ρ, we take 0.133 in view of the prediction by the dispersion relation [10]. We also calculate the cases of $\sigma_t=100$ and 105 mb with $\rho=0.135$ and 0.133, respectively, in order to examine the energy variation of the basic physical quantities between the $Sp\overline{p}S$ and the LHC. The results for the elasticity and the forward slope are given in Table IV. The forward slope is approaching the MacDowell-Martin unitarity bound $B_{MM}\equiv(1+\rho^2)\sigma_t/18\pi x$ [24] crossing down over the black disk value $B/B_{MM}=9/8$ around the LHC energy, but the Chou-Yang model will turn to the black disk limit asymptotically [25].

The predicted differential cross sections at 14 TeV are given in Fig. 2. We note two features of the differential cross section. The first is the change of the curvature structure of the foward peak which was taken by Block *et al.* [17] as one of criteria for the onset of the asymptopia. In order to see this we plot in Fig. 3 the calculated cross section divided by the exponential one $d\sigma/dt=\{d\sigma/dt\}|_{t=0}\exp(Bt)$ where B is the logarithmic slope at $t=0$. The results clearly show the change of the curvature structure around $\sigma_t=100$ mb from concave to convex, where the elasticity x is about 0.28. We will observe the convex feature of the differential cross section at the LHC. The second feature is the appearance of rather clear dip-bump structure at the LHC. In the region 0.5–1.8 TeV the dip of the contribution from the imaginary part of the scattering amplitude is nearly filled up by its real part, but at the LHC there will appear a rather clear dip structure at $|t|=0.4$ (GeV/c)^2, although the value of ρ does not change much from those in the $Sp\overline{p}S$-Tevatron energy [26].

V. TWO-COMPONENT CHOU-YANG MODEL AND THE BOUNDS FOR THE GLUONIC RADIUS OF THE PROTON

The Chou-Yang model in its orginal simple picture, however, does not explain the observed behavior of pp and $\overline{p}p$ scattering if allied to the energy region below the $Sp\overline{p}S$ energy. We need to generalize it by taking two components

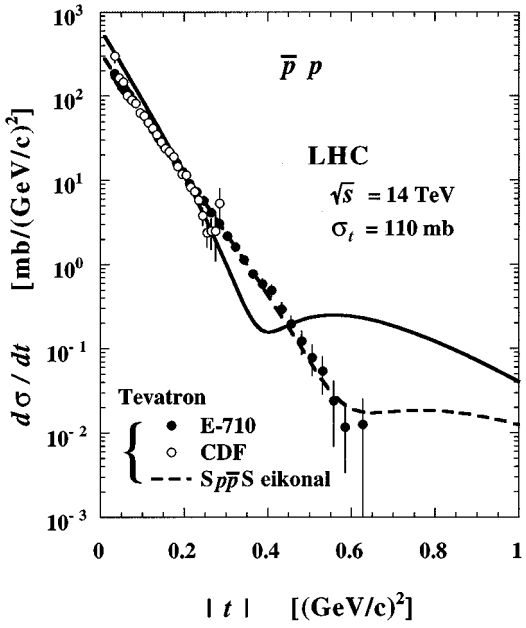

FIG. 2. The differential cross sections of $\overline{p}p$ scattering at 14 TeV calculated by the $Sp\overline{p}S$ eikonal determined from the UA4 and UA4/2 experiments at 0.541–0.546 TeV [20]. The differential cross sections at 1.8 TeV are also shown.

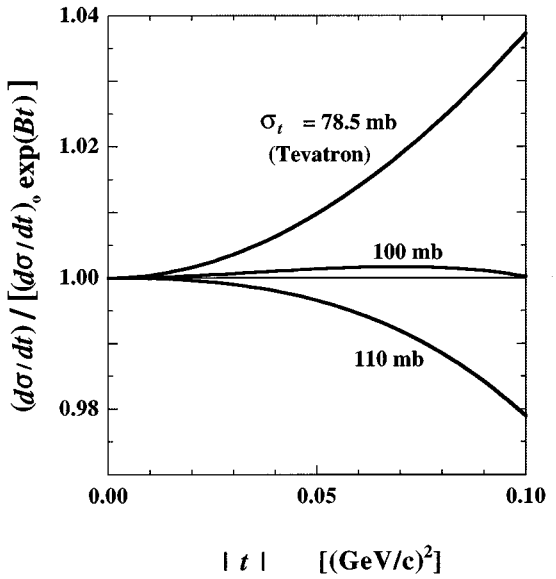

FIG. 3. The change of the curvature structure of the forward peak of $\overline{pp}$ scattering with the total cross section σ_t calculated by the S$p\overline{p}$S eikonal determined from the UA4 and UA4/2 experiments at 0.541–0.546 TeV [20]. We show the ratio of the differential cross section to $d\sigma/dt=\{d\sigma/dt\}|_{t=0}\exp(Bt)$ where B is the logarithmic slope at $t=0$.

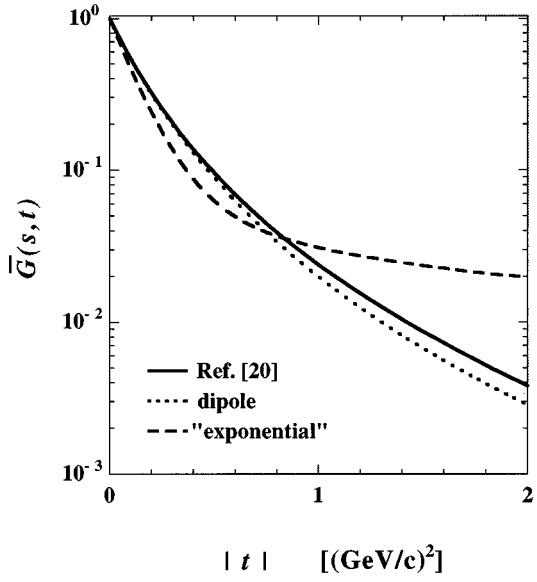

FIG. 4. The function $\overline{G}(s,t)$ of $\overline{pp}$ scattering calculated by the S$p\overline{p}$S eikonal determined from the UA4 and UA4/2 experiments at 0.541–0.546 TeV [20]. For comparison we show those of the exponential cross section and the dipole form factor having the same $d\overline{G}(s,t)/dt|_{t=0}$.

for the hadron constituents, the gluon (g) and the quark (q). The eikonal $\Omega(s,b)$ of the Chou-Yang picture is now written as

$$\Omega(s,b)=W^{qq}(s)G^{qq}(b)+2W^{qg}(s)G^{qg}(b)+W^{gg}(s)G^{gg}(b), \tag{14}$$

where $W(s)^{ij}$ and $G(b)^{ij}$ are the functions depending only on s and b, respectively. In this case the factorizing representation (10) is only approximate unless one single term dominates the right-hand side of Eq. (14).

The picture of the diffraction interaction (14) is essentially the quantum-chromodynamics-inspired model of Block *et al.* [17] where the analysis was focused on the evaluation of the energy dependence of W^{ij} from the information of the inelastic process. We treat W^{ij} and G^{ij} phenomenologically in the present anslysis.

The results in the preceding sections show that only one component dominates in the S$p\overline{p}$S-Tevatron region. It is reasonable to identify this component as the gluon. The function $\overline{G}(s,t)$ obtained from the scattering amplitude at 0.541–0.546 TeV and shown in Fig. 4 is the product of the two gluonic proton form factors $\overline{G}(t)^{gg}_{pp}=[F^g_p]^2$. The root-mean-square (rms) radius $\overline{r_g}$ of the gluon distribution inside the proton is given by

$$\overline{r_g^2}=\langle r^2_{gluon}\rangle_p=\int r^2\rho^g_p(r)d\mathbf{r}=3\frac{d}{dt}\overline{G}^{gg}_{pp}(t)\bigg|_{t=0}, \tag{15}$$

where we can take $\overline{G}(t)^{gg}_{pp}=\overline{G}(s,t)$ in the present case. Hence the effective proton radius can be identified with the gluonic radius and we have

$$\overline{r_g}=0.88\pm0.01 \quad \text{fm} \tag{16}$$

from the S$p\overline{p}$S eikonal. This value is close to the rough estimate by assuming the exponential differential cross section given in Table II.

The observed constancy of the effective radius of the proton in the S$p\overline{p}$S and Tevatron energy range implies that the quark component *is not positively required* from the present experimental data in this energy range. It will be, however, reasonable to consider that the Chou-Yang asymptopia may be *almost realized*, but *not fully* at this energy. If the value of ρ is as large as 0.135 at the S$p\overline{p}$S, this favors nonvanishing κ_d [20], suggesting the contribution from two kinds of constituents with different spatial distributions. The size of the background is crucial to set the bound for the gluonic radius.

Here we estimate the bounds for the gluonic radius when some background exists within the uncertainties of the present experimental data. We assume the background by quark-quark scattering with the quark density distribution

$$\rho^q_p(r)=\frac{1}{4\pi}\frac{\mu_q^3}{2}e^{-\mu_q r}, \tag{17}$$

corresponding to the dipole form factor with mass μ_q.

As for the gluon component we take the density

$$\rho^g_p(r)=\frac{1}{4\pi}\frac{\mu_n^3}{(n+2)!}(\mu_n r)^n e^{-\mu_n r} \qquad (n=0,1,\ldots), \tag{18}$$

where μ_n is a parameter. The rms radius for the distribution (18) is

$$r_{\rm rms}=\sqrt{(n+3)(n+4)}\,\mu_n^{-1}. \tag{19}$$

The form factor corresponding to the density (18) is given by the sum of the multipoles

$$F_p^g(t)=\frac{1}{n+2}\sum_{k=0}^{[(n+1)/2]}{}_{(n-k+1)}C_k\frac{(-1)^k 2^{n-2k+1}}{\left(1-\frac{t}{\mu_n^2}\right)^{n-k+2}}, \tag{20}$$

where [ ] is the Gaussian symbol and ${}_pC_q$'s are the binomial coefficients. For the numerical calculation it is simpler to use the following expression:

$$F_p^g(t)=\frac{1}{n+2}(\cos\alpha)^{n+2}\sin(n+2)\alpha\cot\alpha, \tag{21}$$

with $\alpha\equiv\arctan(\sqrt{-t}/\mu_n)$.

We examine two cases: (C) a central type with $n=0$ and (P) a peripheral type with $n=1$. The second choice (P) is made by considering the possibility that the gluon distribution in the proton may be peripheral as the bag model suggests [27]. Though these densities are not enough to reproduce the very details of the experimental differential cross sections, they can be used to examine the gluonic radius.

With these choices of the gluon distribution we will limit the upper bound for the gluonic radius of the proton from the forward slope of $\overline{G}(s,t)$ which seems fairly well fixed in the region 0.541–1.8 TeV. The lower bound of the gluonic radius is obviously given by the lower end 0.87 fm of the radius (16). For the quark radius of the proton we take 0.835 fm or $\mu_q=0.819$ GeV in view of the electromagnetic form factors of the proton: Borkowski *et al.* gave the electric radius $\langle r_{\rm E}^2\rangle_p^{1/2}=0.84\pm0.02$ fm and the magnetic radius $\langle r_{\rm M}^2\rangle_p^{1/2}=0.83\pm0.09$ fm [14]. For simplicity we neglect the quark-gluon term in Eq. (14), which will lower the upper bound for the gluonic radius.

At the highest energy of the CERN ISR the difference between the pp and $\overline{p}p$ total cross section is very small, indicating that nondiffractive Regge-pole-type contributions may be practically neglected. Hence the allowed maximal contribution from the quark background can be obtained by saturating the pp or $\overline{p}p$ total cross section at the highest ISR energy. We assume that the background contribution is not increasing from the value of W_{pp}^{qq} given by the total cross section of $\overline{p}p$ scattering, 44.12 ± 0.39 mb at $\sqrt{s}=62.3$ GeV [28]. If the magnitude of the contribution of the background decreases, then the upper bound of the gluonic radius is lowered.

The effective radius of the proton is given by

$$\overline{r^2}=\frac{\overline{r_q^2}W_{pp}^{qq}+\overline{r_g^2}W_{pp}^{gg}}{W_{pp}^{qq}+W_{pp}^{gg}}. \tag{22}$$

In Fig. 5 we show $\overline{r_g}$ as the function of the total cross section $\sigma_{\rm t}$ for $\overline{r}=0.89$ fm, which is the upper end of the effective proton radius (16) and hence sets the upper bound for the gluonic radius. There are only little differences between the results from the two choices of the gluonic form factor in this case. There is a clear discrepancy in the total cross section between the E-710 and the CDF experimental data with no overlapping within their standard deviations. We therefore set the allowed region for the total cross section $\sigma_{\rm t}$ by the central values of the two experiments as $72.8\leqslant\sigma_{\rm t}\leqslant80.03$ mb. This gives the value 0.95 fm as the upper bound for the gluonic radius of the proton as seen in Fig. 5. Hence we have the bounds

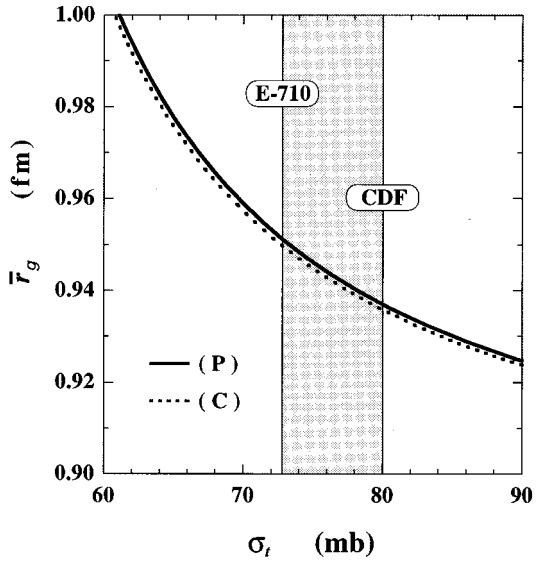

FIG. 5. The shaded area is the allowed region for the gluonic radius $\overline{r_g}$. Here the value of W^{qq} is fixed to reproduce the $\overline{p}p$ scattering total cross section at 62.3 GeV with no other contribution and the value of W^{gg} is determined to give the effective proton radius $\overline{r}=0.89$ fm.

$$0.87\leqslant\overline{r_g}\leqslant0.95\quad\text{fm}. \tag{23}$$

It will be necessary to note how the spatial extension of the background quark distribution affects the upper bound. If the radius of the background is taken to be 0.811 fm of the standard dipole mass of 0.843 GeV, this would tend to increase the upper bound of the gluonic radius. Such a contribution alone, however, cannot reproduce the effective proton radius at the ISR energy. We need a significant contribution from the gluon even at the ISR energy, which subsequently lowers the upper bound. Effectively this is equivalent to taking the quark contribution reproducing the total cross section as well as the forward slope at the highest ISR energy.

On the other hand, if the quark radius of the proton is as large as 0.862 fm given by Simon *et al.* [29] from the reanalysis of their experimental data of the proton charge radius, we cannot apply the present two-component picture to the energy region below the S$p\overline{p}$S. A quark radius as large as 0.862 fm seems to be difficult to reconcile with the simple senario of the diffraction scattering based on the Chou-Yang model at lower energies including the CERN ISR region. If we confine the energy region to the S$p\overline{p}$S and higher, we can no longer reject the radius 0.862 fm for the quark. This, however, decreases the upper bound to lower than that of Eq. (23), if the quark contribution is not increasing in this energy region.

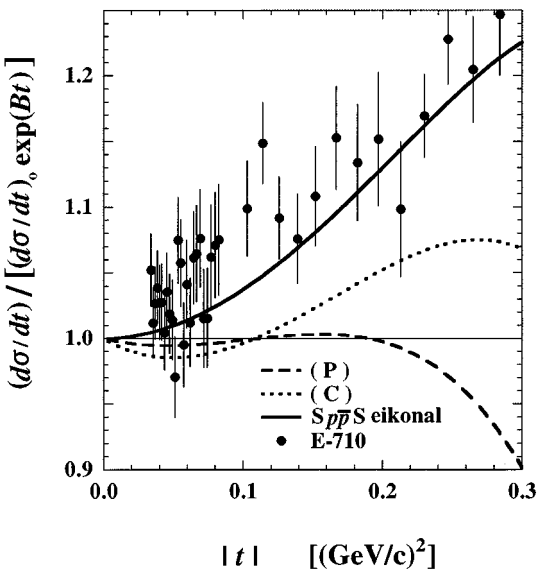

FIG. 6. The differential cross section at 1.8 TeV calculated by the gluon densities (C) and (P) with $\overline{r_g}=0.95$ fm. The quark contribution is of the dipole type with $\mu=0.819$ GeV ($\overline{r_q}=0.835$ fm) and a fixed W^{qq} determined to saturate the $\overline{p}p$ total cross section at 62.3 GeV.

In order to see how the upper bound in Eq. (23) for the gluonic extension affects the differential cross section, we have fitted the differential cross sections in the region $-t \leqslant 0.3$ (GeV/c)^2 for the value of the quark contribution frozen at ISR. Here we restrict the range for the momentum transfer, as the scattering amplitude coming from the simple form (18) can be used only for small momentum transfers. The results at 1.8 TeV are shown in Fig. 6. Here the shape of the gluon density affects the fit. The value of χ^2 of the fit is 194.4 and 57.3 with the data points $N_{\rm DP}=37$, for the peripheral and the central gluon, respectively. For comparison we also show the fit of the *one-component* Chou-Yang model based on the S$p\overline{p}$S eikonal which gives $\chi^2=26.7$ for the same data set. These results show that it is very difficult to reproduce the experimental data of the differential cross section at 1.8 TeV by the gluonic amplitude with radius $\overline{r_g}=0.95$ fm, even though the collaboration of the background term allows the effective proton radius to stay within the experimental uncertainty. The gluonic radius taken by Block *et al.* in their analyses [17] is 0.936 fm and lies near the upper bound of Eq. (23). It is to be noted that they used the quark amplitude with the dipole form factor of the mass of 0.89 GeV, much larger than the standard dipole mass of 0.843 GeV.

VI. PERIPHERALITY OF THE GLUON DISTRIBUTION

For the spatial distribution of the gluon only little experimental information seems to have been obtained so far. Theoretically the bag model [27] provides interesting results which are quoted here. In the MIT bag model [30] the massless-quark density in the ground state of the spherical cavity approximation is [31]

$$\rho_q(r)=N_q\left\{j_0^2\left(\frac{k}{R}r\right)+j_1^2\left(\frac{k}{R}r\right)\right\}. \tag{24}$$

Here R is the bag radius and N_q the normalization factor given by

$$N_q^{-1}=4\pi R^3\frac{2(k-1)}{k(2k^2-2k+1)}, \tag{25}$$

with

$$\tan k=\frac{k}{1-k}. \tag{26}$$

The lowest quark mode is given by $k=2.043$ which leads to $\langle r^2_{quark}\rangle_p^{1/2}=0.73R$ for the massless quark, while we have the gluon distribution in the zero coupling approximation [32] as

$$\rho_g(r)=N_g j_1^2\left(\frac{k'}{R}r\right). \tag{27}$$

Here the normalization factor N_g is

$$N_g^{-1}=4\pi R^3\frac{k'^2-1}{2(k'^4-k'^2+1)}, \tag{28}$$

with

$$\tan k'=\frac{k'}{1-k'^2}. \tag{29}$$

The lowest gluon mode is supplied by $k'=2.744$ which implies $\langle r^2_{gluon}\rangle_p^{1/2}=0.79R$.

In Fig. 7 we show the quark density (24) and the gluon density (27) as well as the interaction profiles given by $G(b)$ for these densities. There is a distinct difference in the two density distributions: The quark distribution is central and the gluon one is peripheral in this model, as the quark ground state has a strong central component from the spherical Bessel function $j_0(kr/R)$, while the gluon one is given by $j_1(k'r/R)$. This is also reflected in the fact that the gluonic radius is larger than the quark one. Apparently the interaction is also more peripheral for the gluon than the quark, but the difference between two cases is much smoothed in the process from the density to the eikonal. These features of the densities are of a kinematical nature in this bag model and will be kept qualitatively for the real proton as far as the MIT-type bag picture has validity, even if effects such as the smooth boundary, excited states, mass center, etc., are introduced.

Here we note some features of the gluon distribution which vanishes at the center as the bag $j_1(k'r/R)$ model: (i) the transformed eikonal $\overline{G(t)}$ has at least one double zero in t and (ii) the eikonal $G(b)$ of the gluon contribution is of a peripheral nature.

The bag-model gluon distribution (27), with its sharp boundary, is not realistic and not suitable for examining possible effects of these features to the actual differential cross section. Therefore, we take simple, but more realistic densities (C) (this is the dipole case) and (P), and calculate the

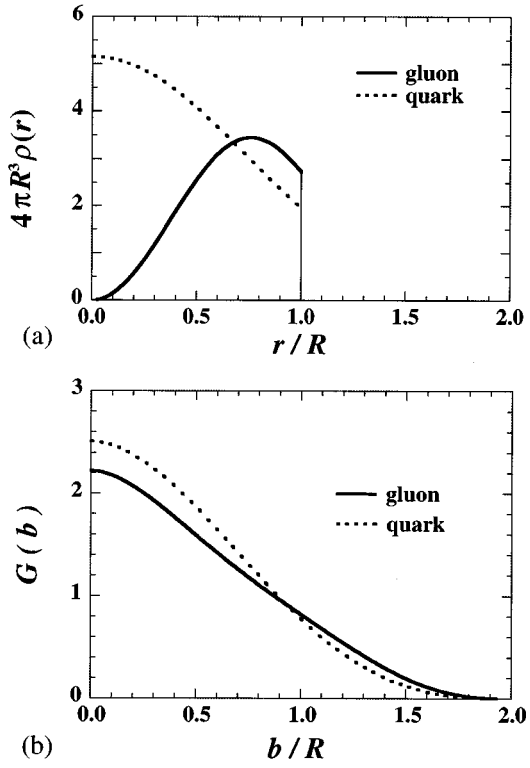

FIG. 7. (a) The quark density (24) and the gluon density (27) of the bag model and (b) the eikonal profile functions $G(b)$ corresponding to these densities.

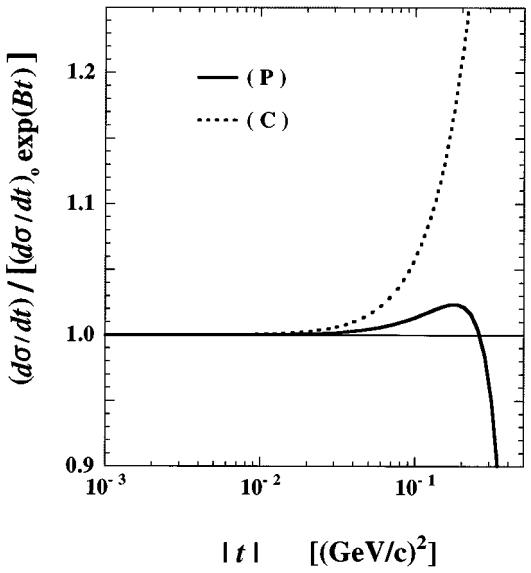

FIG. 8. Comparison of the forward hadronic differential cross sections for two types of the gluon distribution (C) and (P). The mass parameters μ_n and W^{gg} are chosen to reproduce $\sigma_t = 62.2$ mb and $B = 15.5\ (\mathrm{GeV}/c)^{-2}$ and the background term is neglected. The ratios to the differential cross section falling exponentially in the momentum transfer t with the slope $B = 15.5\ (\mathrm{GeV}/c)^{-2}$ are shown.

differential cross section. The form factor corresponding to (C) gives no zero at finite t, while the transformed eikonal $\overline{G(t)}$ for (P) has a double zero at $|t| = 3\mu_1^2$. The scattering amplitude for (P), however, has no clear trace of the double zero, and both show similar diffraction patterns for the values of parameters which reproduce the total and elastic cross section data in the energy region under consideration [33].

As for the second feature, the change of the forward curvature structure of the differential cross section from positive to negative will appear earlier for the form factor of peripheral type (P) than that of central type (C), which occurs commonly as $W(s)$ increases. In Fig. 8 we show the differential cross sections for the distributions (C) and (P) at small $|t|$. Such a peripherality of the gluon distribution might be related to a rather simple behavior of the forward peak of the UA4/2 data falling nearly exponentially in $|t|$ at small momentum transfers $|t| \lesssim 0.1\ (\mathrm{GeV}/c)^2$ [11].

Finally we note that the geometrical scaling behavior of pp scattering in the ISR region [3,36] and the generalized geometrical scaling behavior of pp and $\overline{pp}$ scattering in the ISR to the Tevatron region [4,5] may be approximately realized by the collaboration of two components, the decreasing *shorter-range* quark contribution and the increasing *longer-range* gluon one with the energy, though the ordinary Reggepole contributions are necessary to reproduce the details of the ISR data. The CERN Large Hadron Collider will give us valuable information for establishing the picture of the diffraction dynamics including confirmation of the features obtained in the present analysis.

[1] T.T. Chou and C.N. Yang, Phys. Rev. **170**, 1591 (1968).
[2] See, for example, M.M. Block and R.N. Cahn, Rev. Mod. Phys. **57**, 563 (1985).
[3] U. Amaldi and K.R. Schubert, Nucl. Phys. **B166**, 301 (1980).
[4] M. Kawasaki, T. Maehara, and M. Yonezawa, Phys. Rev. D **47**, R3 (1993); **48**, 3098 (1993).
[5] M. Kawasaki, T. Maehara, and M. Yonezawa, Phys. Rev. D **53**, 4838 (1996).
[6] CDF Collaboration, F. Abe *et al.*, Phys. Rev. D **50**, 5550 (1994).
[7] CDF Collaboration, F. Abe *et al.*, Phys. Rev. D **50**, 5518 (1994).
[8] L. Lewin, *Polylogarithms and Associated Functions* (North-Holland, Amsterdam, 1981).
[9] UA4 Collaboration, M. Bozzo *et al.*, Phys. Lett. **147B**, 392 (1984).
[10] UA4/2 Collaboration, C. Augier *et al.*, Phys. Lett. B **315**, 503 (1993).
[11] UA4/2 Collaboration, C. Augier *et al.*, Phys. Lett. B **316**, 448 (1993).
[12] E-710 Collaboration, N.A. Amos *et al.*, Phys. Rev. Lett. **68**, 2433 (1992).
[13] E-710 Collaboration, N.A. Amos *et al.*, Phys. Lett. B **243**, 158 (1990).

[14] F. Borkowski *et al.*, Nucl. Phys. **A222**, 269 (1974); Nucl. Phys. **B93**, 461 (1975).

[15] For the derivative dispersion relation see J.B. Bronzan, G.L. Kane, and U.P. Sukhatme, Phys. Lett. **49B**, 227 (1974); J.D. Jackson, in *Proceedings of Fourteenth Scottish Universities Summer School in Physics*, 1973, edited by R.L. Crawford and R. Jennings (Academic Press, London, 1974), p. 1.

[16] A. Martin, Lett. Nuovo Cimento **7**, 811 (1973).

[17] M. Block, R. Fletcher, F. Halzen, B. Margolis, and P. Valin, Phys. Rev. D **41**, 978 (1990); M.M. Block, F. Halzen, and B. Margolis, Phys. Lett. B **252**, 481 (1990).

[18] L. Durand III and R. Lipes, Phys. Rev. Lett. **20**, 637 (1968).

[19] H. Cheng, J.K. Walker, and T.T. Wu, Phys. Lett. **44B**, 97 (1973); F. Hayot and U.P. Sukhatme, Phys. Rev. D **10**, 2183 (1974).

[20] M. Kawasaki, T. Maehara, and M. Yonezawa, Phys. Lett. B **348**, 623 (1995).

[21] UA4 Collaboration, R. Battiston *et al.*, Phys. Lett. **127B**, 472 (1983); UA4 Collaboration, M. Bozzo *et al.*, *ibid.* **155B**, 197 (1985).

[22] E-710 Collaboration, N.A. Amos *et al.*, Phys. Lett. B **247**, 127 (1990); Fermilab Report No. FN 562 [E710], 1991 (unpublished).

[23] See, for example, A. Bueno and J. Velasco, Phys. Lett. B **380**, 184 (1996).

[24] S.W. MacDowell and A. Martin, Phys. Rev. **135**, B960 (1964).

[25] M. Kawasaki, T. Maehara, and M. Yonezawa, Phys. Rev. D **48**, 4082 (1993); **50**, 4423 (1994).

[26] A clear dip structure appears around $|t|=0.4$ (GeV/c)^2 at the CERN Large Hadron Collider (LHC) energy in most of the theoretical calculations; for example, C. Bourrely, J. Soffer, and T.T. Wu, Z. Phys. C **37**, 369 (1988); M.M. Block, K. Kang, and A.R. White, Int. J. Mod. Phys. A **7**, 4449 (1992); P. Desgrolard, M. Giffon, and E. Predazzi, Z. Phys. C **63**, 241 (1994). An exception is the model by A.F. Martini and M.J. Menon, Phys. Rev. D **56**, 4338 (1997).

[27] For the bag model see, for example, J.F. Donoghue, E. Golowich, and B.R. Holstein, *Dynamics of the Standard Model* (Cambridge University Press, Cambridge, England, 1992).

[28] N. Amos *et al.*, Nucl. Phys. **B262**, 689 (1985).

[29] G.G. Simon, F. Borkowski, Ch. Schmitt, and V.H. Walther, Z. Naturforsch. A **35**, 1 (1980).

[30] A. Chodos, R.L. Jaffe, K. Johnson, C.B. Thorn, and V.F. Weisskopf, Phys. Rev. D **9**, 3471 (1974).

[31] T. DeGrand, R.L. Jaffe, K. Johnson, and J. Kiskis, Phys. Rev. D **12**, 2060 (1975).

[32] E. Golowich, Phys. Rev. D **18**, 927 (1978).

[33] Here we note the zeros of $\bar{\Omega}(s,t)$ of the Chou-Yang model. In the naive Chou-Yang model the eikonal function in the momentum transfer space $\bar{\Omega}(s,t)$ is positive semidefinite and has no simple zero. Our previous analyses in the ISR region indicated a simple zero around $|t|\approx 6$ (GeV/c)^2, however [4,34]. Recently Carvalho and Menon [35] have made an extensive study of this problem and have shown the existence of a zero in the region $|t| = 5$–9 (GeV/c)^2 which is consistent with our previous finding. The existence of the simple zero will require either additional interactions such as the non-Pomeron Reggepole amplitudes or the departure from the parton-parton point interaction in the Chou-Yang picture.

[34] T. Maehara, T. Yanagida, and M. Yonezawa, Prog. Theor. Phys. **57**, 1097 (1977).

[35] P.A.S. Carvalho and M.J. Menon, Phys. Rev. D (to be published).

[36] J. Dias de Deus, Nucl. Phys. **B59**, 231 (1973); A.J. Buras and J. Dias de Deus, *ibid.* **B71**, 481 (1974).